



HAL
open science

An elasto-plastic contact model applied to nanoindentation

Zhi-Qiang Feng, Maria Zei, Pierre Joli

► **To cite this version:**

Zhi-Qiang Feng, Maria Zei, Pierre Joli. An elasto-plastic contact model applied to nanoindentation. *Computational Materials Science*, 2007, 38 (4), pp.807–813. 10.1016/j.commatsci.2006.05.018. hal-00342923

HAL Id: hal-00342923

<https://hal.science/hal-00342923>

Submitted on 31 Oct 2023

HAL is a multi-disciplinary open access archive for the deposit and dissemination of scientific research documents, whether they are published or not. The documents may come from teaching and research institutions in France or abroad, or from public or private research centers.

L'archive ouverte pluridisciplinaire **HAL**, est destinée au dépôt et à la diffusion de documents scientifiques de niveau recherche, publiés ou non, émanant des établissements d'enseignement et de recherche français ou étrangers, des laboratoires publics ou privés.

An elasto-plastic contact model applied to nanoindentation

Zhi-Qiang Feng ^{a,*}, Maria Zei ^b, Pierre Joli ^c

^a *Université d'Évry-Val d'Essonne, Laboratoire de Mécanique d'Évry, 40 rue du Pelvoux, 91020 Évry, France*

^b *Université d'Évry-Val d'Essonne, Laboratoire d'Études des Milieux Nanométriques, Bâtiment de Science, rue Père Gerlan, 91020 Évry, France*

^c *Université d'Évry-Val d'Essonne, Laboratoire IBISC, 40 rue du Pelvoux, 91020 Évry, France*

This paper is devoted to the finite element modeling of the nanoindentation problem. The frictional contact between the Berkovitch indenter and the very thin elasto-plastic film is treated by the bi-potential method. The elasto-plastic constitutive equation is integrated by means of the radial return mapping algorithm and the consistent tangent operator is explicitly derived. Numerical results show the validity of the model.

Keywords: Elasto-plasticity; Contact; Finite element analysis; Nanoindentation

1. Introduction

The development of nano-materials used in nanotechnology, for example, assembly of structures, manufacture of nanotubes, etc. requires the knowledge of mechanical properties such as the Young modulus, the yield stress or the buckling loadings. The evaluation by nanoindentation of these properties represents a real challenge for the researchers because it is difficult to carry out experiments at such length scales. Moreover, to validate a experimental result, it is necessary to be ensured of its reproducibility which requires many samples and involves thus a high cost. Different analytical models were proposed in the case of thin metal layers (with elasto-plastic behavior) [1] or polymers (with hyperelastic behavior and pile-up) [2]. The nanoindentation can be very complex because of two principal strongly nonlinear phenomena: elasto-plasticity and contact with friction. In the case where analytical derivation of the mechanical properties is not feasible, numerical modeling may therefore help to clarify and put in evidence the different contributions of thin films and substrates.

Knapp et al. [3] used the FE approach to determine hardness properties of thin films in two dimensions. They suggested a fit procedure to evaluate mechanical properties of thin layers and substrates. This kind of procedure reveals some success but with several limitations: two dimensional geometry, hundred of nanometers length scales, geometrically perfect indenter and the neglecting of interface interactions (film/substrate). For smaller length scale it seems to be necessary to develop more complex interaction film-substrate models, as in the work of Bull et al. [4,5].

The aim of this paper is to develop an three-dimensional elasto-plastic contact model. The purpose is also to investigate and characterize structural and mechanical properties of different coatings with increasing hardness at a length scale of tens of nanometers. Usually, behavior laws of solids are differential equations which connect the rate of stress to the rate of strain. Nagtegaal et al. [6], Hughes and Winget [7] have proposed several integration schemes. The concept of consistent linearization introduced by Nagtegaal [6] and extended by Simo and Taylor [8] made it possible to write, in the case of small or large deformations, effective tangent stiffness matrices. The analysis of contact problems with friction is of great importance in many engineering applications. The numerical treatment

* Corresponding author. Tel.: +33 1 69 47 75 01; fax: +33 1 69 47 75 99.
E-mail address: feng@iup.univ-evry.fr (Z.-Q. Feng).

of the unilateral contact with dry friction is certainly one of the nonsmooth mechanics topics for which many efforts have been made in the past. In the literature, many attempts have been developed to deal with such problems using the finite element method. A large literature base is available for a variety of numerical algorithms [9,10]. The bi-potential method proposed by de Saxcé and Feng [11] has been successfully applied to solve contact problems between elastic or hyperelastic bodies [12,13]. In the present work, this method will be applied to solve the nanoindentation problem involving the contact between the rigid indenter and the elasto-plastic film.

2. Modelling of elasto-plastic materials

At low temperature, or when the loading speeds are relatively low, the metallic materials present inelastic time-independent deformations. The total strain $\boldsymbol{\varepsilon}$ is split into two components: an elastic part $\boldsymbol{\varepsilon}^e$, connected linearly to the stress tensor $\boldsymbol{\sigma}$, and a plastic part $\boldsymbol{\varepsilon}^p$:

$$\boldsymbol{\varepsilon} = \boldsymbol{\varepsilon}^e + \boldsymbol{\varepsilon}^p \quad (1)$$

$$\boldsymbol{\sigma} = \mathbb{D} : \boldsymbol{\varepsilon}^e \quad (2)$$

where \mathbb{D} denotes the fourth-order elasticity tensor.

It is supposed that there is a convex field in the space of stresses inside of which there is no plastic flow. The conditions of the plastic flow can be summarized by the following equations:

$$\text{Elasticity if } f < 0 \quad \text{or} \quad f = 0 \quad \text{and} \quad \frac{\partial f}{\partial \boldsymbol{\sigma}} : \boldsymbol{\sigma} < 0 \quad (3)$$

$$\text{Plasticity if } f = 0 \quad \text{and} \quad \frac{\partial f}{\partial \boldsymbol{\sigma}} : \boldsymbol{\sigma} > 0 \quad (4)$$

where f stands for the yield function and $f=0$ represents the loading surface delimiting the elastic domain. In a general case, the surface of load is represented by an ellipsoid in the stress space. In the case of isotropic plasticity considered here, we use the von Mises criterion as follows:

$$f(\boldsymbol{\sigma}, \mathbf{x}, R) = \sqrt{\frac{3}{2}(\mathbf{s} - \mathbf{x}) : (\mathbf{s} - \mathbf{x})} - R = \sqrt{\frac{3}{2}\boldsymbol{\eta} : \boldsymbol{\eta}} - R \leq 0 \quad (5)$$

where R and \mathbf{x} represent respectively the radius and the center of the elastic domain. $\mathbf{s} = \boldsymbol{\sigma} - \frac{1}{3}\text{tr}(\boldsymbol{\sigma})\mathbf{I}$ is the deviator stress tensor and $\boldsymbol{\eta} = \mathbf{s} - \mathbf{x}$.

In the case of associated plasticity, the principle of normality is written by

$$\dot{\boldsymbol{\varepsilon}}^p = \dot{\lambda} \frac{\partial f}{\partial \boldsymbol{\sigma}} = \dot{\lambda} \mathbf{n} \quad (6)$$

The von Mises stress is given by

$$J(\boldsymbol{\eta}) = \sqrt{\frac{3}{2}\boldsymbol{\eta} : \boldsymbol{\eta}} \quad (7)$$

From Eq. (5), we have

$$\mathbf{n} = \frac{\partial f}{\partial \boldsymbol{\sigma}} = \frac{3}{2} \frac{\boldsymbol{\eta}}{J(\boldsymbol{\eta})} = -\frac{\partial f}{\partial \mathbf{x}} \quad (8)$$

The normality law is expressed then in the form:

$$\dot{\boldsymbol{\varepsilon}}^p = \dot{\lambda} \boldsymbol{\eta} \quad (9)$$

where $\dot{\lambda} = \frac{3}{2J(\boldsymbol{\eta})} \dot{\lambda}$ is the plastic multiplier.

Because the strain and stress tensors are symmetric, vector forms can be used. Let us introduce a diagonal matrix $\mathbf{P} = \text{diag}(1 \ 1 \ 1 \ 2 \ 2 \ 2)$, the yield function can be written in another form as

$$g = \frac{1}{2} \boldsymbol{\eta}^T \mathbf{P} \boldsymbol{\eta} - \frac{1}{3} R^2 \leq 0 \quad (10)$$

The isotropic law of strain hardening is defined by the evolution of the radius R with respect to the cumulated plastic deformation p by

$$R(p) = R_s - (R_s - R_0)e^{-\gamma p} \quad (11)$$

where R_s , R_0 and γ are material constants. R_s represents the saturated radius and R_0 the initial one.

The linear Prager kinematic hardening is defined by the evolution of center \mathbf{x} of the elastic domain with respect to the plastic strain rate:

$$\dot{\mathbf{x}} = \frac{2}{3} H \dot{\boldsymbol{\varepsilon}}^p = \frac{2}{3} H \dot{\lambda} \boldsymbol{\eta} \quad (12)$$

where H is the slope of the kinematic work hardening.

The integration of behavior laws plays a very important role in a finite element code. Indeed, it determines the precision of the solution. Errors on the estimates of the variables, once made, are not retrievable any more, moreover when the estimates depend on the history of the loading these errors can be propagated from an increment to another. The results deviate more and more from the solution. In this study, the implicit integration algorithm has been chosen.

Let us consider a plastically admissible state (corresponding to the load step n) and the known characteristics of this state are: $\boldsymbol{\sigma}_n$, \mathbf{x}_n , p_n verifying $g_n = g(\boldsymbol{\sigma}_n, \mathbf{x}_n, p_n) = 0$.

From an incremental displacement $\Delta \mathbf{u}$, we can calculate the increment of strain:

$$\Delta \boldsymbol{\varepsilon} = \mathbf{B} \Delta \mathbf{u} \quad (13)$$

where \mathbf{B} is an operator derived from shape functions. Integrating constitutive laws consists in calculating: $\boldsymbol{\sigma}_{n+1}$, p_{n+1} , \mathbf{x}_{n+1} , $\boldsymbol{\eta}_{n+1}$ checking:

$$\boldsymbol{\varepsilon}_{n+1}^p = \boldsymbol{\varepsilon}_n^p + \Delta \lambda \boldsymbol{\eta}_{n+1} \quad (14)$$

$$\mathbf{x}_{n+1} = \mathbf{x}_n + \frac{2}{3} H \Delta \lambda \boldsymbol{\eta}_{n+1} \quad (15)$$

$$p_{n+1} = p_n + \sqrt{\frac{2}{3}} \Phi_{n+1} \Delta \lambda; \quad \Phi_{n+1} = \sqrt{\boldsymbol{\eta}_{n+1}^T \mathbf{P} \boldsymbol{\eta}_{n+1}} \quad (16)$$

$$\mathbf{s}_{n+1} = G(\mathbf{e}_{n+1} - \boldsymbol{\varepsilon}_{n+1}^p) \quad (17)$$

$$\boldsymbol{\sigma}_{n+1} = \mathbf{D}(\mathbf{s}_{n+1} - \boldsymbol{\varepsilon}_{n+1}^p) \quad (18)$$

$$\boldsymbol{\eta}_{n+1} = \mathbf{s}_{n+1} - \mathbf{x}_{n+1} \quad (19)$$

The most used method to integrate the laws of plastic behavior is undoubtedly the ‘‘Radial Return Mapping’’ (RRM), initially introduced by Wilkins [14], Krieg and Krieg [15] for models of perfectly plastic behavior. The extension of this method to the case of the models with nonlinear kinematic work hardening was carried out by Simo and Taylor [16]. The principle of this method is to calculate the final stress $\boldsymbol{\sigma}_{n+1}$ as the projection of a test stress $\boldsymbol{\sigma}_E$ onto the yield surface according to the normal passing by $\boldsymbol{\sigma}_E$ (Fig. 1).

The test stress is calculated by supposing that the increment of strain is entirely elastic:

$$\boldsymbol{\sigma}_E = \boldsymbol{\sigma}_n + \Delta\boldsymbol{\sigma}_E = \boldsymbol{\sigma}_n + \mathbf{D}\Delta\boldsymbol{\varepsilon} \quad (20)$$

The relations (14)–(19) are easily carried out as soon as one obtained the plastic multiplier $\Delta\lambda$ defined by the condition of consistency at the end of the step:

$$g(\boldsymbol{\sigma}_{n+1}, \mathbf{x}_{n+1}, p_{n+1}) = 0 \quad (21)$$

Replacing the relations (14)–(19), the Eq. (21) becomes a nonlinear relation in $\Delta\lambda$:

$$g(\Delta\lambda) = 0 \quad (22)$$

2.1. Calculations of $\Delta\lambda$

In view of (16) and (21), we have:

$$g = \frac{1}{2}\boldsymbol{\eta}_{n+1}^T \mathbf{P}\boldsymbol{\eta}_{n+1} - \frac{1}{3}R^2(p_{n+1}) = 0 \quad (23)$$

It leads then to find $\boldsymbol{\eta}_{n+1}$ as a function of $\Delta\lambda$ and of known variables.

By using the relations (14), (17), (19), we obtain:

$$\begin{aligned} \boldsymbol{\eta}_{n+1} &= \mathbf{s}_{n+1} - \mathbf{x}_{n+1} \\ &= G(\mathbf{e}_{n+1} - \boldsymbol{\varepsilon}_{n+1}^p) - \mathbf{x}_n - \frac{2}{3}H\Delta\lambda\boldsymbol{\eta}_{n+1} \\ &= G(\mathbf{e}_{n+1} - \boldsymbol{\varepsilon}_n^p - \Delta\lambda\boldsymbol{\eta}_{n+1}) - \mathbf{x}_n - \frac{2}{3}H\Delta\lambda\boldsymbol{\eta}_{n+1} \\ &= G(\mathbf{e}_{n+1} - \boldsymbol{\varepsilon}_n^p) - \mathbf{x}_n - \left(G + \frac{2}{3}H\right)\Delta\lambda\boldsymbol{\eta}_{n+1} \end{aligned} \quad (24)$$

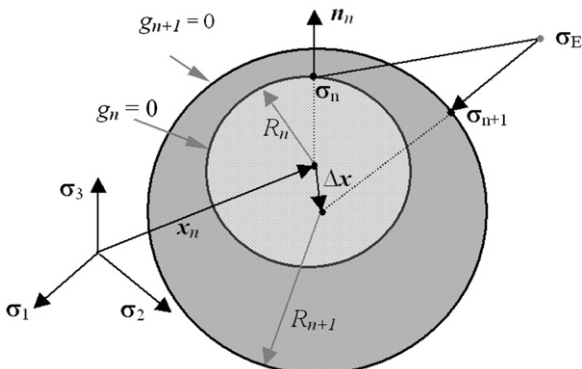


Fig. 1. Radial return mapping.

Posing $\boldsymbol{\eta}_E = G(\mathbf{e}_{n+1} - \boldsymbol{\varepsilon}_n^p) - \mathbf{x}_n$ (which is known), we have

$$\boldsymbol{\eta}_{n+1} = \frac{\boldsymbol{\eta}_E}{1 + \left(G + \frac{2}{3}H\right)\Delta\lambda} \quad (25)$$

Introducing (25) into (23) gives

$$g(\Delta\lambda) = \frac{\boldsymbol{\eta}_E^T \mathbf{P}\boldsymbol{\eta}_E}{2\left(1 + \left(G + \frac{2}{3}H\right)\Delta\lambda\right)^2} - \frac{1}{3}R^2(p_{n+1}) = 0 \quad (26)$$

where $p_{n+1} = p_n + \sqrt{\frac{2\boldsymbol{\eta}_E^T \mathbf{P}\boldsymbol{\eta}_E}{3\left(1 + \left(G + \frac{2}{3}H\right)\Delta\lambda\right)^2}}\Delta\lambda$.

Posing $\Psi(\Delta\lambda) = \frac{\boldsymbol{\eta}_E^T \mathbf{P}\boldsymbol{\eta}_E}{\left(1 + \left(G + \frac{2}{3}H\right)\Delta\lambda\right)^2}$, the relation (26) becomes:

$$g(\Delta\lambda) = \frac{1}{2}\Psi(\Delta\lambda) - \frac{1}{3}R^2\left(p_n + \sqrt{\frac{2}{3}\Psi(\Delta\lambda)\Delta\lambda}\right) = 0 \quad (27)$$

This nonlinear equation in $\Delta\lambda$ can be solved by the Newton–Raphson method.

2.2. Calculation of the consistent tangent matrix

The consistence condition states that the variation of the criterion is null at the end of the loading step:

$$dg = d\left(\frac{1}{2}\Phi_{n+1}^2 - \frac{1}{3}R^2\right) = \Phi_{n+1}d\Phi_{n+1} - \frac{2}{3}RR'dp_{n+1} = 0 \quad (28)$$

According to (16) we have:

$$dp_{n+1} = \sqrt{\frac{2}{3}}\Delta\lambda d\Phi_{n+1} + \sqrt{\frac{2}{3}}\Phi_{n+1}d(\Delta\lambda) \quad (29)$$

and then:

$$\Phi_{n+1}d\Phi_{n+1} - \frac{2}{3}RR'\left(\sqrt{\frac{2}{3}}\Delta\lambda d\Phi_{n+1} + \sqrt{\frac{2}{3}}\Phi_{n+1}d(\Delta\lambda)\right) = 0 \quad (30)$$

Starting from this condition, we can obtain the consistent tangent matrix as follows:

$$\mathbf{D}_{ep} = \frac{\partial\boldsymbol{\sigma}_{n+1}}{\partial\boldsymbol{\varepsilon}_{n+1}} = \mathbf{A} + \frac{K - G}{3}\mathbf{J} \quad (31)$$

where K and G are the bulk modulus and shear modulus, ($\mathbf{J}_{ij} = 1$ for $i, j = 1, 2, 3$; $\mathbf{J}_{ij} = 0$ for $i, j = 4, 5, 6$) and

$$\mathbf{A} = G\mathbf{I} - \frac{\mathbf{P}\boldsymbol{\eta}_{n+1}\boldsymbol{\eta}_{n+1}^T}{w\Phi_{n+1}^2} \quad \text{with } w = \left(1 + \frac{2(H + R')}{3G(1 - \frac{2}{3}R'\Delta\lambda)}\right) \quad (32)$$

The method of the radial return mapping is equivalent to the pure implicit method which checks the criterion of plasticity at the end of the step and maintain its properties of unconditional stability.

3. Modelling of contact problems

3.1. Contact kinematics

In the section, we describe basic definitions and notations used in contact theory. Two deformable bodies \mathcal{B}^α (Fig. 2), $\alpha = 1, 2$, are considered. Each of them occupies the open, simply connected, bounded domain $\Omega^\alpha \subset \mathbb{R}^3$, whose generic point is denoted \mathbf{X}^α . Furthermore, the solids are elastic and undergo large displacements. The boundary Γ^α of each body is assumed to be sufficiently smooth everywhere such that an outward unit normal vector, denoted by \mathbf{n}^α , can be defined at any point M on Γ^α . At each time $t \in \mathbf{I}$, where $\mathbf{I} = [0, T]$ denotes the time interval corresponding to the loading process, the boundary Γ^α of the body \mathcal{B}^α can, in general, be split into three parts: Γ_u^α with prescribed displacements $\bar{\mathbf{u}}^\alpha$, Γ_t^α with prescribed boundary loads $\bar{\mathbf{t}}^\alpha$, and the potential contact surfaces Γ_c^α where the two bodies \mathcal{B}^1 and \mathcal{B}^2 may possibly come into contact at some time t :

$$\Gamma^\alpha = \Gamma_u^\alpha \cup \Gamma_t^\alpha \cup \Gamma_c^\alpha \quad (33)$$

The successive deformed configurations of \mathcal{B}^α are described at each time t by the displacement fields \mathbf{u}^α defined on $\bar{\Omega}^\alpha$ (i.e. the closure of Ω^α). On the contact surface, a unique normal \mathbf{n} directed towards \mathcal{B}^1 ($\mathbf{n} \equiv \mathbf{n}^2$) is defined and the tangential plane, orthogonal to \mathbf{n} in \mathbb{R}^3 , is denoted by \mathbf{T} . To construct an orthonormal local basis, two unit vectors \mathbf{t}_x and \mathbf{t}_y are defined within the plane \mathbf{T} . For describing the frictional contact interactions that may occur on Γ_c , we introduce the relative velocity with respect to \mathcal{B}^2

$$\dot{\mathbf{u}} = \dot{\mathbf{u}}^1 - \dot{\mathbf{u}}^2 \quad (34)$$

where $\dot{\mathbf{u}}^1$ and $\dot{\mathbf{u}}^2$ are the instantaneous velocities of \mathcal{B}^1 and \mathcal{B}^2 , respectively. Let \mathbf{r} be the contact force distribution exerted on \mathcal{B}^1 at M from \mathcal{B}^2 . According to the action–reaction principle, \mathcal{B}^2 is subjected to the stress vector- \mathbf{r} . In the local coordinate system defined by the tangential plane \mathbf{T} and the normal \mathbf{n} , any element $\dot{\mathbf{u}}$ and \mathbf{r} may be uniquely decomposed as

$$\dot{\mathbf{u}} = \dot{\mathbf{u}}_t + \dot{u}_n \mathbf{n}, \quad \dot{\mathbf{u}}_t \in \mathbf{T}, \quad \dot{u}_n \in \mathbb{R} \quad (35)$$

$$\mathbf{r} = \mathbf{r}_t + r_n \mathbf{n}, \quad \mathbf{r}_t \in \mathbf{T}, \quad r_n \in \mathbb{R} \quad (36)$$

3.2. Contact law and friction rule

The unilateral contact law is characterized by a geometric condition of non-penetration, a static condition of

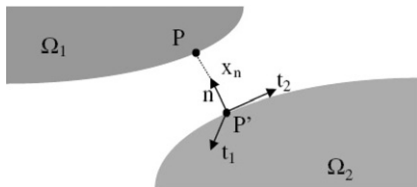


Fig. 2. Projection and gap vector.

no-adhesion and a mechanical complementary condition. These three conditions are known as the Signorini conditions. The non-penetration condition constraints the displacement fields \mathbf{u}^α and is given by

$$g(\mathbf{X}) = (\mathbf{X}^1 - \mathbf{X}^2) \cdot \mathbf{n} \geq 0 \quad (37)$$

where

$$\mathbf{X}^\alpha(t) = \mathbf{X}^\alpha(t=0) + \mathbf{u}^\alpha \quad (38)$$

The position vector \mathbf{X}^2 is found as the closest-point projection of the point $\mathbf{X}^1 \in \Gamma_c^1$ on the surface Γ_c^2 . Denoting by h the initial gap obtained at the beginning of each time step.

$$h = (\mathbf{X}^1 - \mathbf{X}^2) \cdot \mathbf{n} \geq 0 \quad (39)$$

the impenetrability Signorini conditions are given by

$$u_n + h \geq 0, \quad r_n \geq 0, \quad (u_n + h)r_n = 0 \quad (40)$$

These conditions have to be satisfied at each time-instant $t \in \mathbf{I}$. Assume now that the bodies are initially in contact on a certain portion of Γ_c . On this part of Γ_c , the Signorini conditions turn into

$$u_n \geq 0, \quad r_n \geq 0, \quad u_n r_n = 0 \quad (41)$$

In general, at any time $t \in \mathbf{I}$, the potential contact surfaces Γ_c^α can be split into two disjoint parts: $^+\Gamma_c$ where the bodies are already in contact and $^-\Gamma_c$ where the bodies are not in contact:

$$\Gamma_c^\alpha = ^+\Gamma_c \cup ^-\Gamma_c \quad (42)$$

In contrast to Γ_c^α , $^+\Gamma_c$ and $^-\Gamma_c$ change in time t and can be empty at some $t \in \mathbf{I}$. We must stress that with the formulation (41) only a loss of contact is allowed and the extension of the contact area cannot be modelled with these relations. In the case of dynamic analysis such as impact problems, the Signorini conditions can be formulated, on $^+\Gamma_c$, in terms of relative velocity

$$\dot{u}_n \geq 0, \quad r_n \geq 0, \quad \dot{u}_n r_n = 0 \quad \text{on } ^+\Gamma_c \quad (43)$$

When $\dot{u}_n \geq 0$, the bodies are separating while they remain in contact for $\dot{u}_n = 0$. The previous formulation of the Signorini conditions (43) can be combined with the sliding rule to derive the complete frictional contact law applicable on the contacting part of Γ_c . This complete law specifies possible velocities of bodies that satisfy impenetrability, non-adhesion and the sliding rule. Obviously, for a strictly positive gap ($u_n \geq 0$), the normal relative velocity is arbitrary ($\dot{u}_n \in \mathbb{R}$) and the normal reaction force is equal to zero ($r_n = 0$). Motions of bodies that are not in contact are arbitrary until contact is made. This choice is motivated by the fact that the emphasis is put on the definition of admissible evolutions for contacting bodies where the time-integration has to be performed. In the rest of the paper, a “minus” sign will always precede the relative tangential velocity $-\dot{\mathbf{u}}_t$ to emphasize its opposite direction to the friction force.

Classically, a rate independent dry friction law is characterized by a kinematic slip rule. In this work, the classical Coulomb friction rule is used. The set of admissible forces, denoted by K_μ , is defined by

$$K_\mu = \{\mathbf{r} \in \mathbb{R}^3 \text{ such that } \|\mathbf{r}_t\| - \mu r_n \leq 0\} \quad (44)$$

K_μ is the so-called Coulomb's cone and is convex.

3.3. Complete frictional contact law

We consider now the previous friction law embedding an impenetrability condition for completeness. On the contact surface Γ_c , the sliding rule can be combined with the rate form of the Signorini conditions to obtain the frictional contact law that specifies possible scenarios on the contact area (stick, slip, separation). The multivalued nature of this strongly nonlinear law makes problems involving frictional contact among the most difficult ones in solid mechanics. Two overlapped “*if...then...else*” statements can be used to write it analytically:

if $r_n = 0$ then $\dot{u}_n \geq 0$! separating

elseif $\mathbf{r} \in \text{int } K_\mu$ then $\dot{u}_n = 0$ and $\dot{\mathbf{u}}_t = \mathbf{0}$! sticking

else $(\mathbf{r} \in \text{bd } K_\mu \text{ and } r_n > 0)$

$$\left\{ \dot{u}_n \geq 0 \text{ and } \exists \lambda > 0 \text{ such that } -\dot{\mathbf{u}}_t = \lambda \frac{\mathbf{r}_t}{\|\mathbf{r}_t\|} \right\} \text{ ! sliding}$$

endif

(45)

where “ $\text{int } K_\mu$ ” and “ $\text{bd } K_\mu$ ” denote the interior and the boundary of K_μ , respectively. The multivalued character of the law lies in the first and the second part of the statement. If r_n is null then $\dot{\mathbf{u}}$ is arbitrary but its normal component \dot{u}_n should be positive. In other words, one single element of \mathbb{R}^3 ($\mathbf{r} = \mathbf{0}$) is associated with an infinite number of velocity vectors $\dot{\mathbf{u}} \in \mathbb{R}^3$. The same arguments can be developed for the second part of the statement.

4. The bi-potential method

De Saxcé and Feng [11] have shown that the contact law (45) is equivalent to the following differential inclusion:

$$-(\dot{\mathbf{u}}_t + (\dot{u}_n + \mu \|\dot{\mathbf{u}}_t\|)\mathbf{n}) \in \partial \bigcup_{K_\mu} \mathbf{r} \quad (46)$$

where $\bigcup_{K_\mu} \mathbf{r}$ denotes the so-called indicatory function of the closed convex set K_μ :

$$\bigcup_{K_\mu}(\mathbf{r}) = \begin{cases} 0 & \text{if } \mathbf{r} \in K_\mu \\ +\infty & \text{otherwise} \end{cases} \quad (47)$$

The following contact bi-potential is obtained:

$$b_c(-\dot{\mathbf{u}}, \mathbf{r}) = \bigcup_{\mathbb{R}_-} (-\dot{u}_n) + \bigcup_{K_\mu} (\mathbf{r}) + \mu r_n \|\dot{\mathbf{u}}_t\| \quad (48)$$

where $\mathbb{R}_- =]-\infty, 0]$ is the set of the negative and null real numbers.

In order to avoid nondifferentiable potentials that occur in nonlinear mechanics, such as in contact problems, it is convenient to use the Augmented Lagrangian Method [17–19, 11, 20]. For the contact bi-potential b_c , given by (48), provided that $\dot{u}_n \geq 0$ and $\mathbf{r} \in K_\mu$, we have:

$$\forall \mathbf{r}' \in K_\mu, \quad \varrho \mu (r'_n - r_n) \|\dot{\mathbf{u}}_t\| + (\mathbf{r} - (\mathbf{r} - \varrho \dot{\mathbf{u}}))(\mathbf{r}' - \mathbf{r}) \geq 0 \quad (49)$$

where ϱ is a solution parameter which is not user-defined. In order to ensure numerical convergence, ϱ can be chosen as the maximum value of the diagonal terms of the local contact stiffness matrix. Taking account of the decomposition (35) and (36), the following inequality has to be satisfied:

$$\mathbf{r}' \in K_\mu, \quad (\mathbf{r} - \boldsymbol{\tau}) \cdot (\mathbf{r}' - \mathbf{r}) \geq 0 \quad (50)$$

where the modified augmented surface traction $\boldsymbol{\tau}$ is defined by

$$\boldsymbol{\tau} = \mathbf{r} - \varrho (\dot{\mathbf{u}}_t + (\dot{u}_n + \mu \|\dot{\mathbf{u}}_t\|)\mathbf{n}) \quad (51)$$

The inequality (50) means that \mathbf{r} is the projection of $\boldsymbol{\tau}$ onto the closed convex Coulomb's cone:

$$\mathbf{r} = \text{proj}(\boldsymbol{\tau}, K_\mu) \quad (52)$$

For the numerical solution of the implicit equation (52), Uzawa's algorithm can be used, which leads to an iterative process involving one predictor-corrector step:

$$\text{Predictor } \boldsymbol{\tau}^{i+1} = \mathbf{r}^i - \varrho^i (\dot{\mathbf{u}}_t^i + (\dot{u}_n^i + \mu \|\dot{\mathbf{u}}_t^i\|)\mathbf{n}) \quad (53)$$

$$\text{Corrector } \mathbf{r}^{i+1} = \text{proj}(\boldsymbol{\tau}^{i+1}, K_\mu)$$

It is worth noting that, in this algorithm, the unilateral contact and the friction are coupled via the bi-potential. Another gist of the bi-potential method is that the corrector can be analytically found with respect to the three possible contact statuses: $\boldsymbol{\tau} \subset K_\mu$ (contact with sticking), $\boldsymbol{\tau} \subset K_\mu^*$ (no contact) and $\boldsymbol{\tau} \subset \mathbb{R}^3 - K_\mu \cup K_\mu^*$ (contact with sliding). K_μ^* is the polar cone of K_μ . This corrector step is explicitly given as follows:

if $\mu |\boldsymbol{\tau}_t^{i+1}| < -\boldsymbol{\tau}_n^{i+1}$ then $\mathbf{r}^{i+1} = \mathbf{0}$! separating

elseif $|\boldsymbol{\tau}_t^{i+1}| < \mu \boldsymbol{\tau}_n^{i+1}$ then $\mathbf{r}^{i+1} = \boldsymbol{\tau}^{i+1}$! sticking

else $\mathbf{r}^{i+1} = \boldsymbol{\tau}^{i+1} - \frac{(\|\boldsymbol{\tau}_t^{i+1}\| - \mu \boldsymbol{\tau}_n^{i+1})}{(1 + \mu^2)} \left(\frac{\boldsymbol{\tau}_t^{i+1}}{\|\boldsymbol{\tau}_t^{i+1}\|} + \mu \mathbf{n} \right)$! sliding

(54)

5. Global solution algorithm

Generally, nonlinear mechanical behaviors of solid media, discretized by N_e finite elements are governed by a set of equilibrium equations:

$$\mathbf{F}_{\text{int}}(\mathbf{u}) - \mathbf{F}_{\text{ext}} - \mathbf{R} = \mathbf{0} \quad (55)$$

where \mathbf{F}_{ext} is the vector of external loads, \mathbf{R} the vector of contact forces in the global coordinate frame. The vector of internal forces $\mathbf{F}_{\text{int}}(\mathbf{u})$ is calculated by

$$\mathbf{F}_{\text{int}}(\mathbf{u}) = \bigwedge_{e=1}^{N_e} \mathbf{F}_{\text{int}}^e(\mathbf{u}) \quad (56)$$

with

$$\mathbf{F}_{\text{int}}^e(\mathbf{u}) = \int_{V^e} \mathbf{B}^T \boldsymbol{\sigma}(\mathbf{u}) dV \quad (57)$$

The symbol \bigwedge denotes a standard finite element assembly operator. The solution of Eq. (55) is obtained by using the Newton–Raphson iterative procedure:

$$\begin{cases} \mathbf{K}_T^i \Delta \mathbf{u}^i = \mathbf{F}_{\text{ext}} + \mathbf{R}^i - \mathbf{F}_{\text{int}}^i(\mathbf{u}^i) \\ \mathbf{u}^{i+1} = \mathbf{u}^i + \Delta \mathbf{u}^i \end{cases} \quad (58)$$

where \mathbf{K}_T is the global tangent stiffness matrix:

$$\mathbf{K}_T = \bigwedge_{e=1}^{N_e} \mathbf{K}_T^e \quad (59)$$

The tangent stiffness matrix \mathbf{K}_T^e for each element is obtained by taking the derivative of $\mathbf{F}_{\text{int}}^e$ with respect to the nodal displacements \mathbf{u} . In addition, by using Eqs. (31) and (57), we obtain

$$\mathbf{K}_T^e = \frac{\partial \mathbf{F}_{\text{int}}^e(\mathbf{u})}{\partial \mathbf{u}} = \int_{V^e} \mathbf{B}^T \mathbf{D}_{\text{ep}} \mathbf{B} dV \quad (60)$$

6. Numerical application

The elasto-plastic contact model described above has been implemented in an in-house finite element program. In this study, the nanoindentation problem is solved with the program. A tetrahedral indenter of Berkovitch type comes in contact onto a thin layer surface (thickness of 300 nm) on a substrate. The thin layer is supposed to have an elasto-plastic behavior. The indenter is supposed to be rigid with a blunted point of radius of curvature of approximately 50 nm. Fig. 3 shows the model with a grid in 3D as well as a more detailed view in 2D. It should be noted that the symmetry of the model is taken into account in order to reduce the computing time. We needed to have a triangular base pyramid with the tip rounded. The tip of the indenter has been created with a 3D animation program (LIGTH-

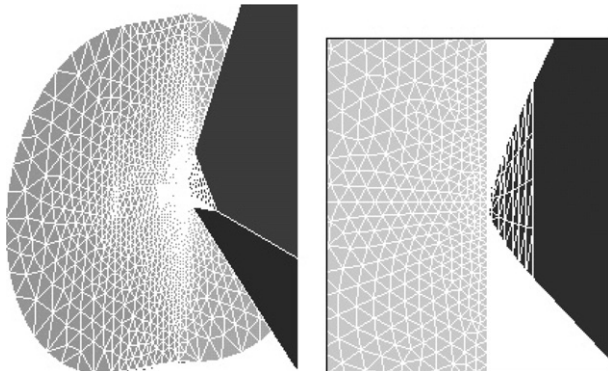


Fig. 3. 3D and 2D view of the mesh.

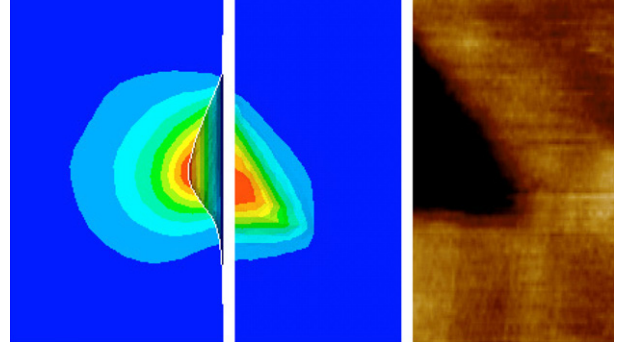


Fig. 4. Numerical and experimental results.

WAVE 7.5). It has several special features that have allowed us to realize the rounded tip with a radius of 50 nm with a tolerance of 2% as shown in Fig. 3. Then we have realized a mesh on this 3D object. The mesh of the film and the substrate are generated by the finite element code ANSYS. We have chosen an appropriate level of meshing to have the minimum number of contact elements between the tip and our meshed material, as we can see in Fig. 3.

Fig. 4 shows the print left on the surface and the distribution of stresses around the zone of indentation. The triangular form of the print accurately reproduces what we observe in experiments on this scale.

7. Conclusion

We have carried out a finite element model at a nano-length scale in the case of an analysis of nanoindentation properties for metal thin films. The elasto-plastic model with contact reveals to be also powerful for treating this kind of simulation at smaller length scales. We confronted the numerical results obtained with experimental measurements of the mechanical behaviors taken on monolithic films, by taking account of the real and imperfect form of the tip. We obtained a good agreement such as the print left on surface and distribution of stress around the zone of indentation. The extension of the model is to perform nanoindentation on multi-structured films. The model will be then developed to take into account the interaction at interfaces between different layers. Recent works suggest to couple the finite element model with a molecular dynamic model to study material behavior at different length scales [21,22]. So we plan to apply this model for the modeling of scratch indentation tests and fracture problems.

References

- [1] W.C. Oliver, G.M. Pharr, *J. Mater. Res.* 7 (1992) 1564–1583.
- [2] J.L. Bucaille, S. Stauss, E. Felder, J. Michler, *Acta Mater.* 51 (2003) 1663–1678.
- [3] J.A. Knapp, D.M. Follstaedt, S.M. Myers, J.C. Barbour, T.A. Friedmann, *J. Appl. Phys.* 58 (1999) 1460–1474.

- [4] S.J. Bull, E.G. Berasetgui, T.F. Page, *Wear* 256 (2004) 857–866.
- [5] E.G. Berasetgui, S.J. Bull, T.F. Page, *Thin Solid Films* 447–448 (2004) 26–32.
- [6] J.C. Nagtegaal, *Comput. Methods Appl. Mech. Eng.* 33 (1982) 469–484.
- [7] T.J.L. Hughes, J. Winget, *Int. J. Numer. Meth. Eng.* 15 (1980) 1862–1867.
- [8] J.C. Simo, R.L. Taylor, *ASME J. Press. Vess. Piping Div.* 48 (1985) 101–118.
- [9] Z.H. Zhong, *Finite Element Procedures for Contact-impact Problems*, Oxford University Press, Oxford, 1993.
- [10] P. Wriggers, *Computational Contact Mechanics*, John Wiley Sons, 2002.
- [11] G. De Saxcé, Z.Q. Feng, *Math. Comput. Model.* 28 (4-8) (1998) 225–245, Special issue: Recent Advances in Contact Mechanics.
- [12] Z.-Q. Feng, F. Peyraut, N. Labed, *Int. J. Eng. Sci.* 41 (2003) 2213–2225.
- [13] Z.-Q. Feng, P. Joli, J.-M. Cros, B. Magnain, *Comput. Mech.* 36 (2005) 375–383.
- [14] M.L. Wilkins, in: B. Alder, S. Fernbach, M. Retenberg (Eds.), *Methods of Computational Physics*, vol. 3, Academic Press, New York, 1964, pp. 211–263.
- [15] R.D. Krieg, B.D. Krieg, *ASME J. Press. Vess. Piping Div.* 99 (1977) 510–515.
- [16] J.C. Simo, R.L. Taylor, *Int. J. Numer. Meth. Eng.* 22 (1986) 649–670.
- [17] P. Alart, A. Curnier, *Comput. Methods Appl. Mech. Eng.* 92 (1991) 353–375.
- [18] J.C. Simo, T.A. Laursen, *Comput. Struct.* 42 (1992) 97–116.
- [19] G. De Saxcé, Z.Q. Feng, *Mech. Struct. Mach.* 19 (1991) 301–325.
- [20] A. Klarbring, *Mathematical programming and augmented Lagrangian methods for frictional contact problems*, in: A. Curnier (Ed.), *Proc. Contact Mechanics Int. Symp.*, PPUR, 1992.
- [21] Z.-Q. Feng, M. Zei, P. Joli, in: M. Lahmani, C. Bréchinac, P. Houdy (Eds.), *Nanosciences 2: Nanomatériaux et Nanochimie, Partie B, Chapitre IX, La Nanomécanique, Modélisation*, Belin, 2006.
- [22] Z.-Q. Feng, M. Zei, P. Joli, *Dix Moins Neuf – La revue des nanosciences et des nanotechnologies, Techniques de l'Ingénieur* 3 (2006) 47–59.